Implementation of Spherical Mode Filtering Based Reflection Suppression Through the Use of the Generalized Vector Addition Theorem for Antenna Position Translation

S.F. Gregson [1,2], M. Dirix [3,4], F. Reher [4]
[1] Next Phase Measurements LLC, CA, USA, stuart.gregson@qmul.ac.uk
[2] Queen Mary University London, London, UK
[3] Emerson & Cuming Anechoic Chambers, Belgium
[4] Institute of High Frequency Technology, RWTH Aachen University, Germany

***Abstract*—In many cases, reflections within antenna test ranges can be the most significant single source of measurement uncertainty within the range assessment budget. Frequency domain, monochromatic, mode-filtering based techniques have become an indispensable tool in the antenna metrologists arsenal providing a very effective method for supressing range multi-path effects resulting from parasitically coupled re-radiation in all forms of modern free-field antenna measurements. These techniques rely upon the acquisition of the test antenna when offset from the origin of the measurement coordinate system. Thus, during the post-processing, it is required that the antenna be translated back to the origin of the measurement coordinate system which has, until very recently, been performed ubiquitously by applying a differential phase change to the far fields. This paper provides further validation of an alternative strategy involving the use of the generalized vector addition theorem for applying the antenna position translation. As this paper demonstrates, this is especially convenient for the case of spherical near-field measurements as several domain transformations are negated. This paper extends the authors prior studies by comparing the traditional and revised algorithms using empirically gathered spherical near-field data taken in a scattering rich environment.**

***Index Terms— Addition Theorem, Mode Filtering, Reflection Suppression, Spherical Mode Expansion*.**

I. INTRODUCTION

The use of mode filtering to improve the quality of antenna measurements taken in non-anechoic environments is a well-known, highly effective, general-purpose, technique, *cf.* [1, 2, 3, 4, 5, 6] with further confirmation of the wide acceptance being provided by the inclusion of a new clause dedicated to this topic being incorporated within the most recent draft of the 1720-2012 - IEEE Recommended Practice for Near-Field Antenna Measurements, [7]. Typically, this form of reflection suppression processing is applied during the transformation process, with the technique being equally applicable to a wide variety of different antenna types, both high and low gain, with no specific a priori assumptions about the type or structure of antenna under test (AUT) being made. In essence, the processing orthogonalises those fields that are associated with the AUT from those fields associated with other spurious, parasitically coupled, sources. In this way, the unwanted contributions can be effectively filtered out. However, successful processing requires that a larger amount of data be acquired than would otherwise be the case for the measurement of the same antenna when installed centrally within a perfect anechoic environment.

Typically, an antenna is installed within a near-, or far-field facility such that it is displaced in space as little as possible during the course of an acquisition. As range reflections tend to disturb the fields illuminating the test antenna, the purpose of this strategy is to construct a scenario where the total field illuminating the test antenna changes as little as possible during the acquisition. However, in our scenario, we adopt a fundamentally different strategy where the test antenna is deliberately displaced from the centre of rotation, which has the effect of making the differences in the illuminating field far more pronounced than would otherwise be the case. And, it is this greater differentiation that makes their identification and subsequent attenuation feasible. This offset also complicated the phase characteristics of the measured fields requiring a larger number of higher order spherical mode coefficients (SMC) to accurately represent the measured field, and a correspondingly larger minimum sphere radius [6, 8].

For the special case of the spherical near-field measurement application, this processing is a little cumbersome as we must first perform a probe-corrected spherical near-field to far-field transformation, which itself involves the computation of the SMCs, to then be able to compute the translation by means of a phase change to the far-field pattern, after which a further spherical wave expansion and summation are necessitated to implement the mode filtering step. While this approach has been widely applied and validated, it comes at the expense of additional computational processing and can result in some loss of generality due to the requirement to pass through the asymptotic far-field. Thus, the traditional spherical mode-

filtering based reflection suppression algorithm can be summarised as follows:

1. Take the two orthogonal tangential electric spherical near-field components (E_θ, E_ϕ) and perform a spherical wave expansion.
2. Apply probe compensation to the SMCs.
3. Perform a spherical mode summation to obtain the asymptotic far-electric fields.
4. Apply a differential phase change to mathematically translate the AUT back to the origin of the measurement co-ordinate system.
5. Perform a second spherical wave expansion to obtain the SMCs for the translated AUT.
6. Apply two-dimensional mode filtering function to suppress unwanted SMCs.
7. Perform a second spherical wave summation to obtain the far-field pattern for the mode-filtered reflection supressed far-fields.

Conversely, the revised, general-purpose generalized vector addition theorem based algorithm can be expressed as:

1. Take the two orthogonal tangential electric spherical near-field components (E_θ, E_ϕ) and perform a spherical wave expansion.
2. Apply probe compensation to the SMCs.
3. Use the generalised vector addition theorem to mathematically translate the AUT back to the origin of the measurement co-ordinate system.
4. Apply two-dimensional mode filtering function to suppress unwanted SMCs.
5. Perform a spherical wave summation to obtain the far-field pattern for the mode-filtered reflection supressed far-fields.

Thus, the new, rigorous, algorithm can be easily implemented directly within the standard data processing chain of any spherical near-field transformation algorithm without the need to transform through the asymptotic far-field. The remainder of this paper is devoted to obtaining further experimental verification of the revised algorithm. To this end, Section II presents an overview of the use of the generalised vector addition theorem for spherical waves, Section III presents results of the processed empirical data, Section IV utilises the rotation theorem to enable far-field data to be presented in an azimuth over elevation coordinate system and polarisation basis rigorously. The paper finishes by presenting a summary and the conclusions.

II. Translation of Spherical Waves

Consider first two right-handed coordinate systems, one primed, and one unprimed, that are initially coincident and synonymous. Now assume that the unprimed system is fixed with the primed system being displaced by a distance A in a straight line in the direction specified by the conventional right-handed polar spherical angles θ_0, φ_0. It may be shown that the translation of spherical waves can be expressed, when using the formulation of [8] as a linear operation [9] so that the spherical wave function $\vec{F}^{(c)}_{smn}(r,\theta,\varphi)$ can be expressed as a combination of spherical waves defined in the primed system $\vec{F}^{(c)}_{\sigma\mu\nu}(r',\theta',\varphi')$ as [10],

$$\underline{F}^{(c=3)}_{smn}(r,\theta,\phi) = \sum_{\sigma\mu\nu} C^{(c=1)}_{\sigma\mu\nu}(\theta_0,\phi_0,k_0A)\,\underline{F}^{(c=3)}_{\sigma\mu\nu}(r',\theta',\phi') \quad (1)$$

Where the summation is defined as follows,

$$\sum_{\sigma\mu\nu} = \sum_{\sigma=1}^{2}\sum_{\nu=1}^{\infty}\sum_{\mu=-\nu}^{\nu} \quad (2)$$

Here $\vec{F}^{(c)}_{\sigma\mu\nu}(r',\theta',\varphi')$ represent a set of spherical vector wave functions in the primed coordinate system, with $C^{smn(c=1)}_{\sigma\mu\nu}(\theta_0,\varphi_0,kA)$ denoting the translation coefficients with (c) indicating the spherical radial function assuming the conventional 1, 2, 3, and 4, numbering system of [18]. Thus, we choose c = 3 for the spherical vector wave functions before, $\vec{F}^{(c)}_{\sigma\mu\nu}(r',\theta',\varphi')$, and then after the translation, $\vec{F}^{(3)}_{smn}(r,\theta,\varphi)$ in the unprimed coordinate system once the translation operation has been applied, matching the outward travelling wave assumption [11]. In this case, we choose (c) = 1, *i.e.* Bessel functions of the 1st kind within the calculation of $C^{smn(c=1)}_{\sigma\mu\nu}(\theta_0,\varphi_0,kA)$ so that this translation can be applied to either incoming *or* outgoing travelling waves and where equation (1) expresses a generalization of the far-field differential phase change operation described above that includes both propagating and evanescent fields, and that is valid for large and small magnitudes of A. Here, we use A to denote the distance of the physical offset applied to the antenna in the translation operation. Where, the translation coefficients are defined as in [10] and [12]. However, in the open literature, several different normalisations factors have been used within the generation of the spherical wave functions, and thus consistent normalisation needs to be applied to the translation coefficients. While the present work assumes a normalisation as described in [8], the calculated translation coefficients using [9] need to be renormalised by a factor of,

$$\alpha = \sqrt{\frac{\nu(\nu+1)}{n(n+1)}} \quad (3)$$

The next section illustrates the use of the new generalised, rigorous, data processing algorithm with measured data.

III. Measured Results

Up until now, the verification of the revised spherical mode-filtering based reflection suppression algorithm has largely been predicated on the successful use of computational electromagnetic simulations of scattering contaminated spherical measurements [10, 11], and the equivalence of results when compared with the traditional algorithm. In this section we shall repeat the verification, only here we shall use measured data. Thus, empirical measurements were taken in a scattering rich environment. Figure 1 below shows a dual six-axis industrial robotic antenna measurement system being used to acquire an x-band slotted waveguide array (SWGA) antenna in an open workshop environment with no absorber present on the robots or in the test environment, and a large scatterer positioned to one side of the spherical near-field acquisition. This clearly presents a demanding, clutter rich, test environment. The AUT can be seen to the right of the

figure, while the probe can be seen located to the left. The linearly polarised x-band SWGA antenna was acquired at 9.3 GHz in polar spherical mode with a measurement radius of 5.842 m, and an offset distance of 0.325 m in the *z*-axis resulting in a minimum sphere radius (MRE) of 0.6 m. Here, the AUT offset distance was on the order of the size of the radiating aperture of the circular SWGA antenna which is sufficient for effective mode filtering [6]. A data point spacing of 1° in θ, and 5° in ϕ, was used which easily satisfied the spherical sampling theorem.

Fig. 1. Dual robotic antenna measurement system being used to acquire an x-band slotted waveguide array antenna in an open shop environment with no absorber and a large scatterer on one side of the acquisition.

Figure 2 below contains the conventional spherical near-field to far-field transformed copolar and cross-polar amplitude patterns where the field was tabulated on a nadir centred, regular, azimuth over elevation plotting coordinate system, and resolved onto a commensurate Ludwig 2, azimuth over elevation polarisation basis [6]. When inspecting these figures, the scattering artefacts are evident within the copolar pattern in the form of spurious sidelobes at *circa* 50° in azimuth, and on the cross-polar pattern at *circa* 50° in θ in the inter-cardinal, *i.e.* ϕ = ±45°, planes.

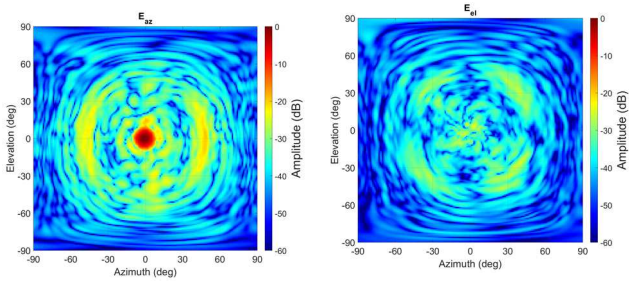

(a) Ludwig 2, Copolar far-field amplitude pattern.

(b) Ludwig 2, cross-polar far-field amplitude pattern

Fig. 2. False colour plot of copolar and cross-polar far-field of slotted waveguide antenna without reflection suppression.

By way of a comparison, Figure 3 presents equivalent far-field plots only here, the new reflection suppression algorithm has been utilised to extract the scattering artefacts. From inspection of these figures, it is very clear that the spurious sidelobes noted in Figure 2 are absent from Figure 3, which is a very encouraging result that can be compared to equivalent data obtained using the traditional reflection suppression algorithm (that in contrast to that which was used here, passes the data via the asymptotic far-field).

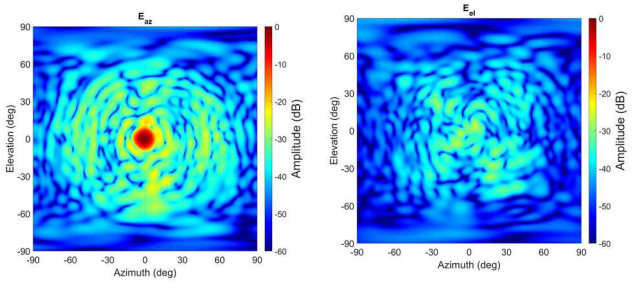

(a) Ludwig 2, Copolar far-field amplitude pattern.

(b) Ludwig 2, cross-polar far-field amplitude pattern

Fig. 3. False colour plot of copolar and cross-polar far-field of slotted waveguide antenna with reflection suppression.

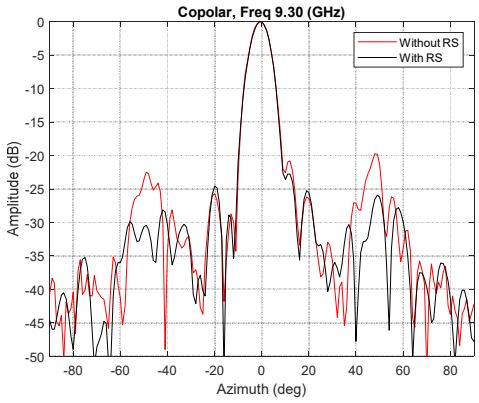

Fig. 4. Azimuth cut comparing copolar amplitude plots without reflection suppression (RS) in red, and with reflection suppression (RS) in black.

The effect of the reflection suppression is further illustrated in Figure 4 which contains a comparison of the azimuth cut comparing copolar amplitude plots without reflection suppression (RS) in red, and with reflection suppression (RS) in black. Figures 5 – 7 presented below illustrate the behaviour of the SMCs as they propagate through the new data processing chain. Figure 5 presents plots of the amplitude of the transverse-electric (TE) and transverse-magnetic (TM) SMCs as computed using a standard spherical mode expansion [6]. These SMCs are then translated using the Generalized Vector Addition Theorem of equation (1) with the resulting TE and TM amplitude plots of the resulting SMCs being presented in Figure 6. Here, SMCs associated with the AUT can be seen located towards the "tip" of the spectrum pattern in the vicinity of lower order *m* and *n* mode indices. Conversely, those modes associated with the scatterer, seen located towards the right-hand side of the plot towards higher *n* indices, have shifted towards higher order modes. This behaviour is as expected and aligns with what we see when implementing this translation using the traditional, far-field, approach. Next, these SMCs were filtered above *n*

$= k_0 r = 30$ where r denotes the conceptual minimum MRE, using a simple low pass filter function [13],

$$Q_{TEmn}\Big|_{\text{Filtered}} = Q_{TEmn} f_m f_n \tag{4}$$

$$Q_{TMmn}\Big|_{\text{Filtered}} = Q_{TMmn} f_m f_n \tag{5}$$

Where,

$$f_m = \begin{cases} 0.5^{(|m|-m_{Max})} & \text{when } |m| > m_{Max} \\ 1 & \text{elsewhere} \end{cases} \tag{6}$$

$$f_n = \begin{cases} 0.5^{(n-n_{Max})} & \text{when } n > n_{Max} \\ 1 & \text{elsewhere} \end{cases} \tag{7}$$

The filtered SMCs can be seen presented in Figure 6 where the spurious higher order SMCs have been attenuated. When these SMCs are summed to obtain the far-field, we obtain the results presented above in Figure 3. In this way we have demonstrated that the use of the general vector addition theorem for SMCs yields the same mode behaviour as the traditional far-field antenna translation approach.

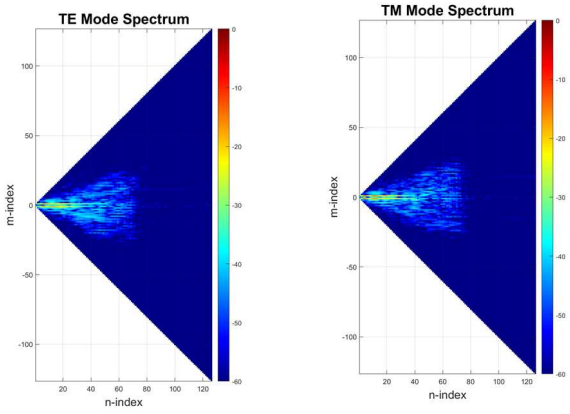

(a) . (b) .

Fig. 5. Mode spectra of the SWGA: (**a**) TE modes; (**b**) TM modes prior to AUT translation.

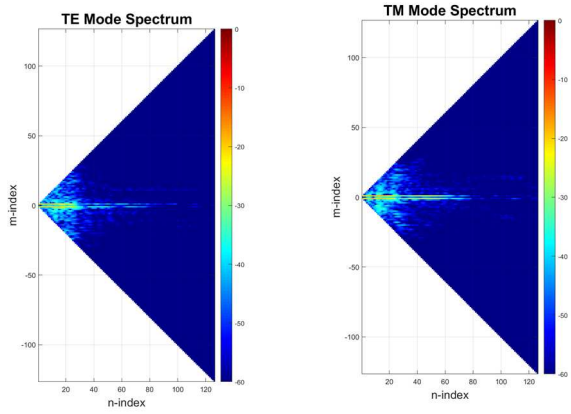

(a) . (b) .

Fig. 6. Mode spectra of the SWGA: (**a**) TE modes; (**b**) TM modes after AUT translation. Here we see the AUT and spurious scattered modes have separated.

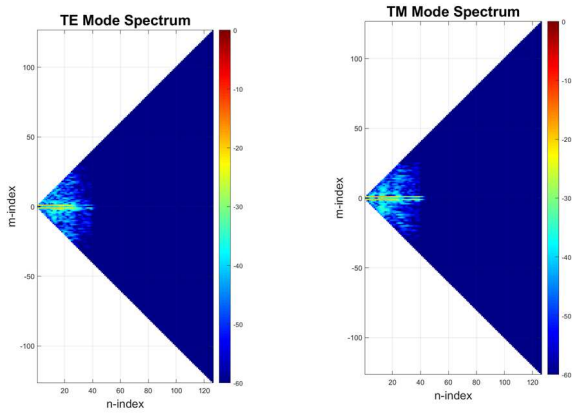

(a) . (b) .

Fig. 7. Mode spectra of the SWGA: (**a**) TE modes; (**b**) TM modes after AUT translation and after the application of the low pass SMC filter.

Figures 8a and 8b present comparison contours, *i.e.* iso-level plots that illustrate the degree of agreement attained between the traditional and new algorithm which implements the AUT translation within the SMC domain. The degree of agreement is sufficiently good that the red contours are not visible as they coincide with the black contours *exactly*.

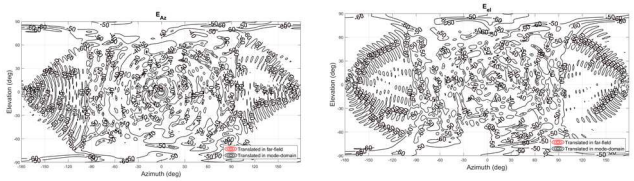

(a) Copolar. (b) Cross-polar.

Fig. 8. Comparison of far-field mode filtered patterns, traditional far-field translation denoted by red contours, translated in mode-domain denoted by black contours.

The degree of agreement between the respective algorithms was further confirmed by computing the dB difference level. Figure 9 contains a false colour checkerboard plot of the dB difference level for the copolar case. From inspection of this we see that the agreement is very encouraging. This is further confirmed by the RMS dB difference level which was approximately -181 dB for the copolar case, and -186 dB for the cross-pol case. These are on the limit of double precision arithmetic and as such represent a very encouraging result.

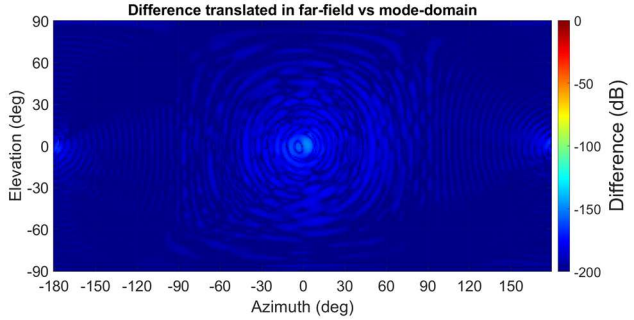

Fig. 9. False colour plot of the dB difference level between mode filtered far-field patterns where the translation of the AUT was performed in the mode domain and in the far-field.

IV. Rotation of Antenna Pattern

It is well known that a rotation operation can be applied to the spherical mode coefficients directly with [14],

$$Q_{smn} = \sum_{\mu=-n}^{n} e^{im\varphi_0} d_{\mu m}^{n} e^{i\mu\chi_0}(\theta_0)\, Q_{s\mu n} \qquad (8)$$

where Q_{smn}, and $Q_{s\mu n}$ are the rotated and unrotated spherical mode coefficients respectively, and θ_0, φ_0, and χ_0 are Euler angles [6]. One of the major advantages of applying rotations to the spherical mode coefficients rather than to the far-field pattern is that the rotation is rigorous, and thus no approximation, *e.g.* interpolation, is necessary. This form of rotation can be applied after the AUT SMCs are filtered and can be used to present the far-field in the form used here in Figures 2, 3, 4, 8, and 9. Thus a key example of the use of this sort of rotation is when SNF data is taken using a ϕ-over-θ positioner stack-up with the antenna boresight direction pointing towards the pole, meaning positive or negative *z*-axis, of the acquisition coordinate system. In this way, the far-field pattern can be tabulated on a regular azimuth over elevation coordinate system and a Ludwig 2 azimuth over elevation polarisation basis by rotating the AUT and relabelling the axes. The necessary Euler angles are θ_0=90°, φ_0=90°, and χ_0=180°. The SMCs for the rotated antenna can be seen presented in Figure 10. Here, it is noted though that an angular rotation may increase the bandwidth requirement of the azimuth (m) modes although the number of N modes remains stable as a rotation does not increase the maximum radial extend of the AUT. Finally, the angular re-mappings are Az = ϕ, and El = 90° - θ, while the polarisation conversion required is $E_{Az} = E_{\phi}$, and $E_{El} = E_{\theta}$.

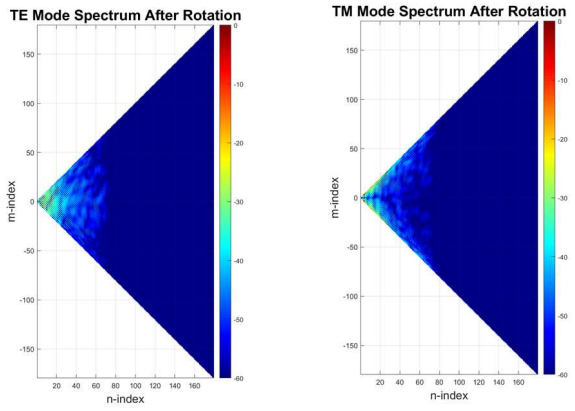

(a) Rotated TE SMCs. (b) Rotated TM SMCs.

Fig. 10. Mode spectra of SWGA: (a) TE modes; (b) TM modes after AUT translation and after filtering and after rotation (from polar-pointing to equatorial-pointing orientation for Az/El presentation), *cf*. Figure 6 above.

V. Summary and Conclusion

This paper extends the validation work that has been reported previously by the authors that further validates the novel, generalised, frequency domain, spherical mode filtering based, scattering suppression technique. This study exploited empirical data to augment the prior studies that exclusively utilised full-wave computational electromagnetic simulations to provide the data required to enable the very precise verification and validation of the new algorithm. Uniquely, this algorithm utilises the generalised spherical addition theorem to implement the requisite antenna translation where translation operation was applied directly to the antenna SMCs and is entirely general since it is not limited to considering just the first order, m =±1 azimuthal modes, but rather is valid for *all* azimuthal modes for which $|m| \le n$. The success of the revised, streamlined, spherical mode filtering bases reflection suppression algorithm is attested to by a comparison with a traditional implementation with agreement being on the order of double precision arithmetic. This provides valuable additional verification for both algorithms and is the first time that this has been reported. Although in this examination, the translation was only applied in the *z*-axis, prior work has verified its use when translations are also required in the *x*- or/and *y*-axes.

References

[1] O. M. Bucci, G. D'Elia, M. D. Migliore, "A General and Effective Clutter Filtering Strategy in Near-Field Antenna Measurements," Microwaves, Antennas and Propagation, IEE Proceedings, vol. 151, no. 3, pp. 227- 235, 21 June 2004.

[2] G.E. Hindman, A.C. Newell, "Spherical Near-Field Self-Comparison Measurements", AMTA 26th Annual Meeting & Symposium, Atlanta, GA, October 2004.

[3] G.E. Hindman, A.C. Newell, "Reflection Suppression in a large spherical near-field range", AMTA 27th Annual Meeting & Symposium, Newport, RI, October. 2005.

[4] G.E. Hindman, A.C. Newell, "Reflection Suppression To Improve Anechoic Chamber Performance", AMTA Europe 2006, Munich, Germany, March 2006.

[5] D.W. Hess, "The IsoFilterTM technique: extension to transverse offsets", Post deadline Submissions, AMTA, Austin, TX, 2006.

[6] C.G. Parini, S.F. Gregson, J. McCormick, D. Janse van Rensburg, T. Eibert, "Theory and Practice of Modern Antenna Range Measurements 2nd Expanded Edition", IET Electromagnetic Waves series 55 ISBN 978-1-83953-126-2, 2021.

[7] IEEE Std 1720™-2012, "IEEE Recommended Practice for Near-Field Antenna Measurements", IEEE Antennas and Propagation Society, 5th December 2012.

[8] F.H. Larsen, "Probe-Corrected Spherical Near-Field Antenna Measurements", Stockholm, Technical University of Denmark, Dept. of Electromagnetic Systems, 1980.

[9] W. C. Chew and Y. M. Wang, "Efficient Ways to Compute the Vector Addition Theorem," Journal of Electromagnetic Waves and Applications, vol. 7, no. 5, pp. 651-665, 1993.

[10] M. Dirix, S.F. Gregson, R.F. Dubrovka, "Use of the Generalized Vector Addition Theorem for Antenna Position Translation for Spherical Mode Filtering Based Reflection Suppression", MDPI Sensors, Submitted June 2025.

[11] M. Dirix, S.F. Gregson, R.F. Dubrovka, "Use of the Generalized Addition Theorem for Spherical Waves for the Reflection Suppression by Spherical Mode Filtering", Antenna Measurement Techniques Association, Tucson, Arizona, USA, November 2025.

[12] W.C. Chew, Y.M. Wang, "Efficient Ways to Compute the Vector Addition Theorem", Journal of Electromagnetic Waves Appl. 1993, 7, 651–665.

[13] S.F. Gregson, A.C. Newell, P.N. Betjes, C.G. Parini, "Verification of Spherical Mathematical Absorber Reflection Suppression in a Combination Spherical Near-Field and Compact Antenna Test Range", AMTA, Austin Texas, USA, 2017.

[14] J. Hansen, Ed., "Spherical Near-Field Antenna Measurements", IET Press, 2008.